The Astrophysical Journal, 699:469–477, 2009 July 1 doi:10.1088/0004-637X/699/1/469

WARPED IONIZED HYDROGEN IN THE GALAXY

J. C. Cersosimo[1,2], S. Mader[3], N. Santiago Figueroa[1,2,4], S. Figueroa Vélez[1], C. Lozada Soto[1], and D. Azcárate[5]
[1] Department of Physics and Electronics, University of Puerto Rico at Humacao, Humacao, PR 00791, USA; juan.cersosimo@upr.edu
[2] Visiting Astronomer, CSIRO Parkes Observatory, New South Wales, Australia
[3] CSIRO Parkes Observatory, New South Wales, Australia
[4] Department of Astronomy, Columbia University, 550 West 120th Street, Mail Code 5246, New York, NY 10027, USA
[5] Instituto Argentino de Radioastronomía, CC No. 5, 1894 Villa Elisa. BsAs, Argentina
Received 2008 February 22; accepted 2009 March 16; published 2009 June 12

ABSTRACT

We report observations of the H166α (ν = 1424.734 MHz) radio recombination line (RRL) emission from the Galactic plane in the longitude range l = 267°–302° and latitude range b = −3.°0 to +1.°5. The line emission observed describes the Carina arm in the Galactic azimuth range from θ = 260° to 190°. The structure is located at negative latitudes with respect to the formal Galactic plane. The observations are combined with RRL data from the first Galactic quadrant. Both quadrants show the signature of the warp for the ionized gas, but an asymmetry of the distribution is noted. In the fourth quadrant, the gas is located between Galactic radii $R \approx 7$ and 10 kpc, and the amplitude of the warp is seen from the midplane to $z \approx -150$ pc. In the first quadrant, the gas is found between $R \approx 8$ and 13–16 kpc, and flares to $z \approx +350$ pc. We confirm the warp of the ionized gas near the solar circle. The distribution of the ionized gas is compared with the maximum intensity H I emission ($0.30 < n_{\rm H\,I} < 0.45$ cm^{-3}) at intervals of the Galactic ring. The ionized material is correlated with the H I maximum intensity in both quadrants, and both components show the same tilted behavior with respect to the mid-Galactic plane.

Key words: Galaxy: disk – Galaxy: structure – ISM: clouds – ISM: structure
Online-only material: color figure

1. INTRODUCTION

Early investigations of the Galaxy's H I emission revealed that it extends well past the solar circle and that in the outer Galaxy the emission is warped systematically from the midplane in the inner Galaxy (Burke 1957; Kerr 1957; Westerhout 1957; Oort et al. 1958). It has also been shown that the H I layer in the Galaxy flares, becoming thicker at larger distances from the Galactic center (Henderson et al. 1982; Kulkarni et al. 1982; Burton & te Lintel Hekkert 1986). More recent studies by Diplas & Savage (1991) and Voskes & Burton (2006) have yielded a more quantitative description of the warp parameters.

From CO (J = 0–1) observations in the range $270° < l < 300°$ and $-5° < b < +5°$, Grabelsky et al. (1987) show the warp of the molecular layer in the Galactic plane in the outer Galaxy. They noted that the Carina arm is the dominant feature in the data. The distribution of the molecular layer outside the solar circle with respect to the CO midplane dips from $z = -48$ to $z = -167$ pc below the $b = 0$ plane, following similar warping of the H I layer. Additional observations in the third quadrant have shown the warping and flaring of the outer disk delineated by molecular clouds. A tendency for third quadrant clouds to fall below the Galactic plane is noted and interpreted as evidence for a warp in the molecular disk (May et al. 1988, 1997). Also, from CO observations of *IRAS* sources, Wouterloot et al. (1990) concluded that the H I layer is substantially thicker than the molecular clouds layer in the inner Galaxy. At distances greater than R_0, and over the range of distances where the *IRAS* clouds are available, the molecular thickness is systematically less than the H I thickness.

Infrared observations (Sodroski et al. 1987; Freudenreich et al. 1994) and star counts yield a systematic variation of the mean disk latitude with longitude (Djorgovski & Sosin 1989). Freudenreich et al. (1994), using data from the Diffuse Infrared Background Experiment (DIRBE) of the *Cosmic Background Explorer* (*COBE*), derived a similar warp for the interstellar dust layer traced by the far-infrared emission, suggesting that the layers of dust and gas are similarly displaced from the Galactic plane. For the emission from old disk stars, which is dominated by near-infrared wavelengths ($\lambda < 5$ μm), a warp is observed, though with smaller amplitude. A search in the region of Puppis (Orsatti 1992) shows a significant number of faint OB stars at 0.5 kpc below the Galactic plane. The study of the distribution of OB stars (Miyamoto et al. 1988) shows that a sample of OB-type stars follows the warp out to the solar circle. In addition, Kaltcheva & Hilditch (2000) confirm the existence of a young group of OB star toward the Galactic anticenter at distances between 0.3 and 2.5 kpc.

Theoretical studies on the origin of galactic warps suggest several methods of interaction between the disc and misaligned nonspherical dark halos (Sparke & Casertano 1988). Another proposed mechanism is the gravitational influence of nearby satellite galaxies (Weinberg 1998; Bailin 2003). Olano (2004) proposes an interaction of the Galactic disk with a transient circumgalactic flow of high-velocity clouds (HVCs) produced by an event of mass transfer from the Magellanic Clouds. Intergalactic accretion flow has been proposed by López-Corredoira et al. (2002), and also interaction with an intergalactic magnetic field has been proposed (Battaner et al. 1990).

The Galactic disk contains several forms of ionized gas. At one extreme, there are two types of widely distributed ionized gases with very low average density that are a part of the general interstellar medium (ISM); the warm ionized medium (WIM) and the hot ionized medium (HIM; McKee & Ostriker 1977; Kulkarni & Heiles 1988). At the other extreme are the ultra compact H II regions. Between them, there exists a variety of H II regions over a wide range of densities and a relatively narrow range of temperatures. Somewhere between these two extremes, an extended low-density (ELD) ionized component appears prevalent within the Galaxy. This component has been referred

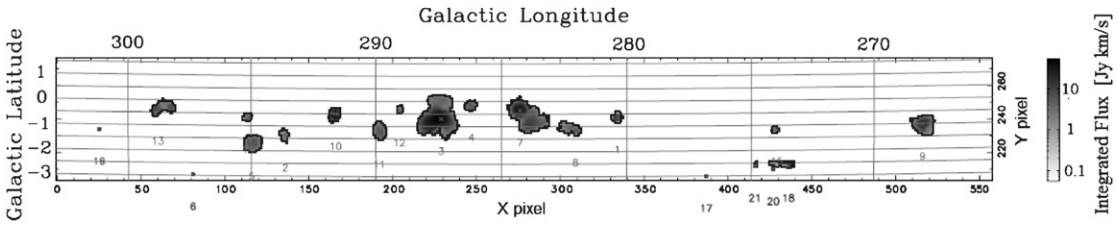

Figure 1. Integrated emission of the H166α line over the interval of Galactic longitude and latitude observed. The grayscale at the right indicates the flux values in units of Jy km s^{-1}.

to as ELD ionized gas by Mezger (1978) and as extended low-density warm ionized medium (ELDWIM) by Petuchowski & Bennet (1993), Heiles (1994), and Heiles et al. (1996).

Although the ELDWIM represents a significant portion of the Galactic ISM, its radial extent as mapped by optical Hα observations is poorly constrained for distances beyond 1–2 kpc from the Sun due to interstellar absorption (i.e., Reynolds 1983). Unrestricted by interstellar absorption, hydrogen radio recombination line (RRL) such as H166α appears sensitive to relatively low-density ($0.5 < n_e < 50$ cm^{-3}) large-angular-sized ionized regions characteristic of the ELDWIM (Brocklehurst & Seaton 1972; Lockman 1976; Cersosimo et al. 1989). Therefore, we can use low-frequency RRL to trace the radial extent of the ELDWIM and detect any warping of the ionized gas layer in the outer Milky Way.

High surface temperature stars such as OB-type are sources of strong ultraviolet (UV) radiation; in the vicinity of these stars the hydrogen is ionized by photons shortward of 912 Å. Since the lifetime of an H II region is relatively short (Osterbrock 1989), we can assume that the stars ionizing the hydrogen gas are hot main-sequence stars (HMSS). The ionized gas would be maintained by the flux of UV radiation coming from hot OB stars, and as a consequence, we can assume that these type of stars are associated with the ELDWIM. Thus, the trace of the ELDWIM, if warped, should represent indirect evidence of the presence of main-sequence (MS) OB-type stellar objects, also warped.

Azcárate et al. (1990) reported the first detection of warped H166α line emission from the Galactic range $270° < l < 300°$. Another observation from the northern hemisphere (Azcárate et al. 1997) noted a flaring of the H166α line emission in the first quadrant. We have now observed H166α (high signal-to-noise ratio) in the fourth quadrant for $267° \leqslant l \leqslant 302°$, $-3.^\circ0 \leqslant b \leqslant +1.^\circ5$.

This paper presents the results of new RRL observations of the southern hemisphere performed with the 64 m antenna of the Parkes Observatory, New South Wales, Australia. The results obtained are displayed as an (l, b) map in Figure 1 and, after the calculation of the kinematic distances and combination with published results for the northern hemisphere, as a Galactic (azimuth, z-height) plot in Figure 5. The Galactic azimuth is defined by the relation $\sin(\theta)/r = \sin(l)/R$, where r and R are the distance from the Sun and the galactocentric distance, respectively, and l is the Galactic longitude. The azimuthal angle θ is defined as being zero on the Sun–center line at large R toward $l = 0°$, and 180° at large R toward $l = 180°$. In the first and second Galactic quadrants, $0° \leqslant \theta \leqslant 180°$; while in the third and fourth quadrants, $180° \leqslant \theta \leqslant 360°$.

2. THE OBSERVATIONS

The region $l = 267° \leqslant l \leqslant 302°$ and $b = -3.^\circ0 \leqslant b \leqslant +1.^\circ5$ was mapped at the H166α line frequency (1424.734 MHz). The receiver used was the Parkes multibeam (Stavely-Smith et al. 1996), a 13-beam receiver package mounted at the prime focus of the Parkes Radiotelescope. The inner 7 beams are packed in a hexagonal configuration with a beam separation on the sky of 29.′1. On-the-fly mapping was performed by scanning the telescope at a rate of 1° minute^{-1} in R.A., recording spectra every 5 s.

The data were recorded in 512 channels across a 4 MHz bandwidth, giving a channel width of 7.8 kHz ($\Delta v = 1.6$ km s^{-1}). The frequency switching mode was used to allow for robust bandpass correction. We switched every 5 s between center frequencies of 1423.5 and 1425.0 MHz. Bandpass calibration was performed using the Livedata package that also performed the Doppler correction to shift the spectra to the kinematic local standard of rest (LSR). Absolute brightness temperature calibration was checked nightly against $\alpha = 19^{\rm h}{:}34^{\rm m}$, $\delta = -6°38'$ (J2000) and Hydra A. The calibrated spectra were gridded into a data cube using the Gridzilla package of the Australia Telescope National Facility (ATNF). The gridding algorithm used in Gridzilla is described in detail in Barnes et al. (2001). The effective resolution of the gridded data is 16′. The per channel rms in the resulting cube is 28 mK. The data have not been corrected for stray radiation.

3. OBSERVATIONAL RESULTS

Figure 1 shows the integrated emission of the H166α line observed in the longitude interval from $l = 267°$ to 302° and $b = -3°$ to $+1.^\circ5$. The map was obtained with the Duchamp program (a source finder program produced at the ATNF; M. Whiting 2007, private communication), which looks into a data cube to obtain the profile of a source. This demonstrated that sources numbers 1, 6, 16, 17, 18, 19, 20, and 21 are not real. These are omitted from Table 1 which contains the description of each source; Column 1 gives the source number, Column 2 the Galactic name, and Column 3 the integrated flux of the line emission. Columns 4 and 5 give the peak intensity of the line and LSR velocity. Column 6 gives the signal-to-noise ratio. Columns 7 and 8 give the longitude and latitude full width of the source, and Column 9 the half power line width (HPLW) of the source. The range of the velocities of the emission detected lies between −30 and +50 km s^{-1}. In terms of kinematic distances, the sources are confined to a distance range not larger than 10 kpc from the Sun.

Comparison of the RRL survey of Caswell & Haynes (1987; hereafter CH) shows a good correlation between H166α and H109α line emission distributions. Furthermore, our 1.4 GHz survey shows the ELDWIM distribution which is present associated with dense H II regions (Roshi & Anantharamaiah 2001). A gap in the sources distribution is found between $l = 270°$ and 274°, and $l = 275°$ and 280°. Many intense sources are located between 280° and 295°. The main area of emission comes from the Carina region, around

Table 1
H166α Emission

Number	G-Name	$F_{\rm int}$ (Jy km s^{-1})	$F_{\rm peak}$ (Jy beam^{-1})	V (km s^{-1})	S/N$_{\rm max}$	ΔGLon ($'$)	ΔGLat ($'$)	ΔV (km s^{-1})
9	267.965−01.029	9.2×10^3	0.83	+5.38	49.70	62.58	47.15	50.96
15	274.026−01.184	47.3	0.21	+38.18	12.45	20.33	15.84	23.02
8	282.202−01.093	1.2×10^3	0.26	+5.02	15.39	56.04	35.94	39.45
7	284.095−00.507	6.5×10^4	1.02	+0.00	61.03	100.02	88.04	65.76
4	286.229−00.174	377.0	0.26	−19.89	15.41	32.01	28.07	32.88
3	287.558−00.705	2×10^5	1.35	−21.16	80.78	100.13	108.42	73.97
12	289.046−00.339	27.8	0.17	+19.34	10.03	16.04	20.09	18.08
11	289.839−01.189	1.4×10^3	0.23	+17.99	16.60	32.17	44.25	37.81
10	291.632−00.540	3.3×10^3	0.90	+8.80	53.86	28.21	36.23	72.33
2	293.648−01.367	115.71	0.17	−24.39	9.88	24.39	36.29	18.08
5	294.941−01.697	2.5×10^3	0.35	−17.12	20.87	44.83	40.52	36.16
14	295.136−00.652	73.6	0.20	+35.95	11.86	24.40	20.26	21.37
13	298.618−00.347	2.7×10^3	0.37	+27.05	22.15	61.70	44.81	44.39

Note. The parameters are obtained with the Duchamp program.

Galactic coordinates G287−1 with an extension of about 3 deg^2.

4. DISTANCE DETERMINATION

One of the relevant parameters needed to understand the structure of the Galaxy is the distance. This is also the most difficult parameter to estimate with accuracy. We obtained the distance by the kinematical method using the peak velocities of the H166α line observations over each integrated profile.

The rotation velocity Θ around the Galactic center of an object at galactocentric distance R, Galactic longitude l, and with radial velocity $V_{\rm LSR}$, is given by

$$\Theta = \frac{R}{R_0}\left(\Theta_0 + \frac{V_{\rm LSR}}{\sin l}\right), \quad (1)$$

where R_0 and Θ_0 denote, respectively, the galactocentric distance and the rotation velocity of the Sun. We adopt the values $\Theta_0 = 220$ km s^{-1} and $R_0 = 8.0$ kpc (Reid 1993). All distances used in this paper are scaled to $R_0 = 8.0$ kpc. If the rotation curve, $\Theta(R)$, is known, Equation (1) allows us to derive R from radial velocity measurements. We have used the linear expression; $\Theta = (221.64 - 0.44R)$ km s^{-1} derived by Fich et al. (1989), and assumed that it holds for galactocentric distances between 3 and 17 kpc. This rotation curve was parameterized for $R_0 = 8.5$ kpc (Fich et al. 1989), while adopting a value of $R_0 = 8.0$ kpc. A smaller value for R_0 results in a slightly steeper rotation curve (Burton 1988; Fich et al. 1989); however, this does not introduce significant errors.

The rotation model of the Galaxy assumes circular rotation. The Sun's path around the Galactic center is called the solar circle. Beyond the solar circle, the velocities continuously decrease or increase without distance ambiguity. Inside the solar circle, the line of sight intersects any galactocentric circle twice; the component of velocity along the line of sight is identical at each intersection because the two points are rotating around the Galactic center with the same angular velocity. Hence, with this model and for the Galactic longitude range studied, the profiles with negative velocities have a distance ambiguity. The most useful data are the photometric measurements for stars associated with the nebulae.

The velocities of the profiles were obtained from Gaussian fits to them (see Table 1). We then obtained the distance from the Sun (r) for the sources. Using these distances, we obtained the Galactic coordinates of the line emission X, Y, where they are defined to be $X = r \cos l$ and $Y = r \sin l$. We also computed the vertical position with respect to the formal Galactic plane, z, which is defined by, $z = r \sin b$. In this reference system, the Sun is at the origin, the X-axis points toward the Galactic center, and the Y-axis points toward longitude $l = 90°$.

The mean error of the $V_{\rm LSR}$ is 3 km s^{-1}, but random motions and superposition of ionized gas along the line of sight add a significant uncertainty to the computed values of the distance errors. The errors on the derived values of r are typically between 10% and 50% depending on the width of the integrated profile obtained with the Duchamp program.

The results are summarized in Table 2. Columns 1 and 2 give the source number and Galactic name of a source. Column 3 gives the central velocity of the profile. Column 4 gives the full width to half intensity $\Delta V_{\rm LSR}$. Column 5 gives the distance. Columns 6–8 give the computed values of the (X, Y, z) Galactic coordinates. Column 9 shows the distance to the center of the Galaxy, and column 10 the Galactic azimuth.

5. DISCUSSION OF INDIVIDUAL SOURCES

CH observed RRLs at 5 GHz for $210° \leqslant l \leqslant 360°$, with a $4'$ beam. We compare their results with ours. Because the optical depth of the line depends on the frequency, the spatial correlation of the sources detected at high and low frequencies should imply the existence of a density gradient (Lockman & Brown 1978) in the H II regions. Furthermore, we searched for a correlation with the optical objects published in the RCW catalog (Rodger et al. 1960).

G267.965–01.029. The integrated profile is obtained from an area of $63' \times 47'$. Inspection of the profiles from the data cube shows the peak velocities of the emission between +0.5 and +9 km s^{-1}. CH observed emission with velocities between +1 and +8 km s^{-1}. The kinematical distance suggests that the ionized gas is located between 0.3 and 2.6 kpc. The optical counterparts are RCW38 and RCW36. In the same region, Kaltcheva & Hilditch (2000) noted a group of OB stars in a distance range from 0.2 to 3 kpc, in agreement with the distance we obtain for the ionized gas. We suggest that the ionized gas is associated with these OB stars. There are also molecular clouds associated with the complex (May et al. 1997) suggesting that

Table 2
Results of Distance Analysis

Number	G-Name	V (km s^{-1})	ΔV (km s^{-1})	r (kpc)	X (kpc)	Y (kpc)	z (pc)	R_G (kpc)	θ (°)
9	267.965−01.029	+5.38	51.0	1.5 ± 1.2	−0.05 ± 0.04	−1.50 ± 1.20	−26 ± 5	8.2 ± 0.1	190.5 ± 9
15	274.026−01.184	+38.18	23.0	6.1 ± 0.3	0.43 ± 0.02	−6.01 ± 0.30	−124 ± 9	9.7 ± 0.1	218.1 ± 2
8	282.202−01.093	+5.02	39.5	4.1 ± 0.8	0.87 ± 0.17	−4.01 ± 0.83	−78 ± 5	8.2 ± 0.1	209.3 ± 5
7	284.095−00.507	+0.00	65.8	3.9 ± 0.5[a]	0.95 ± 0.12	−3.78 ± 0.48	−35 ± 4	8.0 ± 0.2	208.2 ± 4
4	286.229−00.174	−19.89	32.9	2.3 ± 0.4[b]	0.64 ± 0.11	−2.21 ± 0.38	−7 ± 5	7.7 ± 0.2	196.7 ± 3
3	287.558−00.705	−21.16	74.0	2.4 ± 0.2[c]	0.72 ± 0.08	−2.29 ± 0.19	−30 ± 8	7.6 ± 0.2	197.5 ± 2
12	289.046−00.339	+19.34	18.1	7.1 ± 0.3	2.32 ± 0.10	−6.71 ± 0.28	−42 ± 3	8.8 ± 0.1	229.7 ± 3
11	289.839−01.189	+17.99	37.8	7.1 ± 0.4	2.41 ± 0.14	−6.68 ± 0.38	−147 ± 12	8.7 ± 0.1	230.11 ± 3
10	291.632−00.540	+8.80	72.3	6.7 ± 0.7	2.47 ± 0.26	−6.23 ± 0.65	−63 ± 5	8.3 ± 0.1	228.5 ± 6
2	293.648−01.367	−24.39	18.1	3.3 ± 0.5[b]	1.32 ± 0.22	−3.02 ± 0.46	−78 ± 6	7.3 ± 0.2	204.4 ± 4
5	294.941−01.697	−17.12	36.2	2.1 ± 0.4[d]	0.88 ± 0.17	−1.90 ± 0.36	−62 ± 5	7.4 ± 0.1	195.0 ± 3
14	295.136−00.652	+35.95	21.4	9.9 ± 0.3	4.21 ± 0.12	−8.96 ± 0.27	−112 ± 7	9.7 ± 0.1	247.3 ± 6
13	298.618−00.347	+27.05	44.4	9.9 ± 0.4	4.74 ± 0.19	−8.69 ± 0.35	−60 ± 3	9.3 ± 0.1	249.4 ± 6

Notes.
[a] Far distance.
[b] Tangent point.
[c] Photometric distance by Tapia et al. (1988).
[d] Near distance.

star formation is still ongoing in this direction. According to the four-arm model of Russeil (2003), the sources do not belong to the Carina arm.

G274.026–01.184. H109α line emission was reported by CH at this position. The radial velocities of H109α and H166α lines are similar but with different velocity widths. The line width is 33 km s^{-1} at 5 GHz and 23 km s^{-1} at 1.4 GHz. The associated optical source is RCW42.

G282.202–01.093. This source is located within an area of 0.56 deg^2. The integrated profile shows a median radial velocity of −5 km s^{-1} and a width of 39.45 km s^{-1}. Inspection of the RRL reported by CH shows emission with velocities ranging between −1 and +19 km s^{-1}. Inspection of our profiles shows variations of the peak velocity of ±6 km s^{-1}. We suggest a distribution of the emission along the line of sight between 3.4 and 5.1 kpc. The RRL coincides with RCW45.

G284.095–00.507. The integrated profile has an average velocity $v = 0$ km s^{-1} and an HPLW of 65.8 km s^{-1}. The peak velocities of the individual profiles are in the range from about −3 to +3 km s^{-1}. The velocities reported by CH vary from −18 to +16 km s^{-1}. Some components are associated with the optical sources RCW48 and RCW49. We use the velocity obtained from the integrated profile and adopt the far distance $r = 3.9$ kpc (Tsujimoto et al. 2007). The error bar in Figure 2 indicates the spread of the gas along the line of sight.

G286.229–00.174. This has a 0.°5 extension on the sky and a radial velocity of −19.89 km s^{-1}. There is a source detected by CH (G286.195−0.163) with a velocity of −18 km s^{-1}. We conclude that the RRL emission at 5 and 1.4 GHz arises from the same source.

G287.558–00.705. This source covers an area of ∼3 deg^2. Its optical counterpart is NGC 3372 (the Carina nebula), a giant diffuse nebula in one of the largest of H II regions. The optical catalog of Rodger et al. (1960) reports an extended (210′ × 210′) optical source, RCW53. Two radio continuum peaks within the nebula have been reported before (Gardner et al. 1970; Huchtmeier & Day 1975). The width of the profiles suggests that internal motions are present in the region (McGee & Gardner 1968). The V_{LSR} of the integrated profile is −21.16 km s^{-1}, a value 10 km s^{-1} higher than the velocity of the tangent point in the kinematical model. Adopting a tangential point location, the kinematical distance is $r = 2.4$ kpc. This result is in agreement with the photometric distance measured by Tapia et al. (1988), who obtained $r = 2.4 \pm 0.2$ kpc for the clusters embedded into the nebula.

G289.046–00.339. The narrowness of the integrated profile, $\Delta V = 18.08$ km s^{-1}, suggests a low temperature. The kinematic distance is 7.1 ± 0.3 kpc. The emission is also reported by Wilson et al. (1970).

G289.839–01.189. The size of the source is about 32′ × 44′. The integrated profile has radial velocity of ∼18 km s^{-1} and a width of ∼38 km s^{-1}. CH noted four sources, three of these having radial velocities of +22 km s^{-1} and the other +17 km s^{-1}. The distance obtained is 7.1 ± 0.4 kpc.

G291.632–00.540. The integrated profile is from a region of 0.°5 × 0.°6. The optical source projected on this area is RCW57. Our measurements indicate a radial velocity of +8.8 km s^{-1}, yielding a distance of 6.7 ± 0.7 kpc. CH report emission with radial velocities ranging from +9 to +15 km s^{-1}. Other emission was reported from the same sky area by Wilson et al. (1970) and by CH with negative velocity (−25 and −23 km s^{-1}, respectively).

G293.648–01.367. The source size is of about 0.°5 in diameter and has an HPLW of ∼18.1 km s^{-1}. The radial velocity of −24.4 km s^{-1} exceeds the terminal velocity by 6 km s^{-1}. Hence, we assign a distance of 3.3 kpc corresponding to the terminal velocity. Taking into account the change of scale for the Galaxy from $R_0 = 10$ to 8 kpc, the distance assigned is in agreement with that of CH. The source seems to be associated with the optical source RCW60.

G294.941–01.697. This source has an angular diameter of 44′ on the sky. The radial velocity of the integrated profile is −17 km s^{-1}. CH detected two RRL sources at G294.837−01.775 and G295.06−1.650, with radial velocities of −18 km s^{-1} and −22 km s^{-1}, respectively. The optical source RCW62 also lies in the same direction. We assume that all emission belongs to the

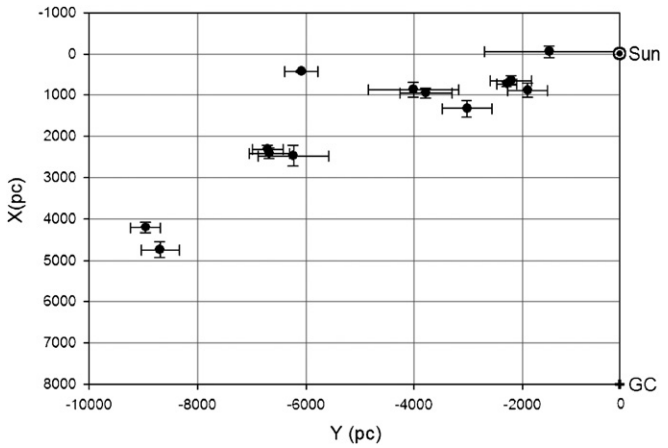

Figure 2. Plot of the RRL emission at the (X, Y) coordinates of the Milky Way; $X = r \cos l$ and $Y = r \sin l$. The error bars are derived from the mean error of the velocity measurements, the random motions, and the superposition of ionized clouds along the line of sight.

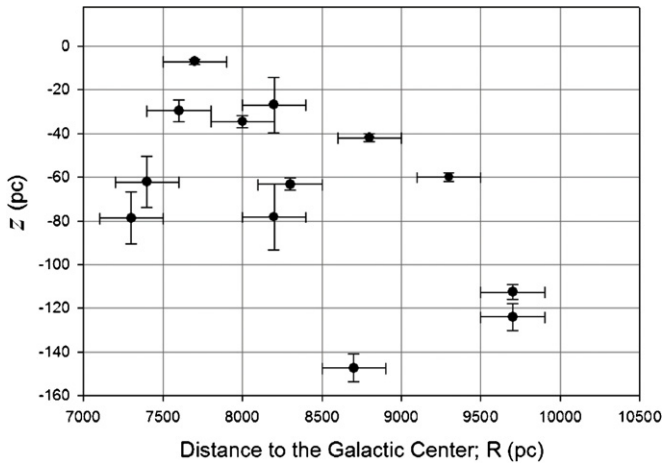

Figure 3. Distribution of the emission sources from Table 2. The axes of the plot represent the distance to the Galactic center vs. z. The tilt of the distribution is the signature of the warp. R_0 is assumed to be 8.0 kpc (Reid 1993).

same complex. The kinematical model suggests two probable distances, and we adopt the near one, $r = 2.1$ kpc.

G295.136–00.652. The small size of the source is superimposed on H109α line emission noted by CH. The radial velocities of both observations agree within the observational errors.

G298.618–00.347. The velocity of the H166α line is +27 km s^{-1} and has HPLW of 44.4 km s^{-1}. From the same area ($62' \times 43'$), CH detect emission at five different positions with radial velocities in the range from +16 to +31 km s^{-1}.

6. THE WARP OF THE IONIZED GAS

Azcárate et al. (1990) present tentative evidence for warped ionized gas in the southern part of the Milky Way. The current observations improve on their data. Figure 3 shows the z-height (z) as a function of Galactic radius (R); the RRL emission appears below the Galactic plane between distances $R =$ 7–10 kpc, and the distribution shows a tilt which descends toward larger R. At larger galactocentric radii, the shape of the distribution reflects that of the warp. The emission goes from the Galactic plane toward greater negative z reaching $z \approx -150$ pc near $R = 10$ kpc. It is apparent that the gas layer is inclined by $\sim 2.^{\circ}8$ toward lower latitudes for larger R. The presence of a low-density ionized gas layer warped in the southern Galaxy has been previously suggested (Azcárate et al. 1990) and is confirmed by the present observations.

6.1. The North and South RRL Emissions

In order to have a more complete view of the behavior of the ionized gas, we have combined our observations with the northern H166α RRL of Azcárate et al. (1997). These observations were obtained within the region $60^{\circ} < l < 87^{\circ}$, $-2^{\circ} < b < +5^{\circ}$. We also included additional observations from $84^{\circ} \leqslant l \leqslant 90^{\circ}$ by Heiles et al. (1996).

Figure 4 (upper panel) shows the l–b distribution of the velocity-integrated H I-peak brightness published by Freudenreich et al. (1994). The two boxes indicate the region where the H166α RRLs were detected at the north by Azcárate et al. (1997) and the region observed in the present survey (south). The lower panels of Figure 4 show the southern (left) and northern (right) regions, which refer to the longitude ranges indicated by the boxes of the upper panel. Dots represent the positions of RRL emission and empty squares represent the integrated H I emission of Freudenreich et al. (1994).

In the lower (left) panel of Figure 4, we show the H166α and the integrated H I distributions $260^{\circ} \leqslant l \leqslant 300^{\circ}$. They seem to be tilted toward lower latitudes from high to lower longitudes. The distribution of the H166α appears significantly above the H I. We will return to this point later.

In the lower (right) panel of Figure 4, we show the data for the ionized gas within $60^{\circ} \leqslant l \leqslant 91^{\circ}$ (Azcárate et al. 1997; Heiles et al. 1996). The integrated H I emission (Freudenreich et al. 1994) appears flat and tilted. The tilt occurs from $b = +2^{\circ}$ at $l = 90^{\circ}$, to $b = 0^{\circ}$ at $l = 60^{\circ}$. Ionized gas seems to be associated with this structure between $l = 83^{\circ}$ and 60°. Below this structure (shown by empty squares) we find ionized gas, distributed above and below the Galactic plane, in the longitude range from $l = 87^{\circ}$ to $l = 70^{\circ}$.

Around $l = 82^{\circ}$ there is a feature above the Galactic plane. The Cygnus superbubble (Landecker 1984) lies in this area of the sky, a region extending $18^{\circ} \times 13^{\circ}$ along the Galactic plane, and was first detected by Cash et al. (1980). Uyaniker et al. (2001) suggest that the bubble was created by OB associations. The region is rich in tracers of recent star formation overlapping along the line of sight. Proper motion measurements by *Hipparcos* confirm the large anomalous velocities of these OB associations. The magnitude and spatial arrangement of the expanding motion (Comerón et al. 1998) suggest that an energetic phenomenon is present in the region.

6.2. The R–θ Plot Distribution

We combine in Table 2 our data set with the distance to the Sun r, the galactocentric distance R, and the Galactic azimuth θ of the H166α sources from Azcárate et al. (1997) and Heiles et al. (1996), all inside the ring $7 < R < 13$ kpc.

In Figure 5, we summarize the results for the fourth and first quadrants. This figure describes the behavior of the ionized gas in (θ, z) coordinates. In the fourth quadrant, a tilted distribution seems to be present from $\theta = 190^{\circ}$ to 250°. In the first quadrant, within the azimuthal range $130^{\circ} < \theta < 180^{\circ}$, and z range $z \pm 100$ pc, the ionized gas is distributed almost symmetrically with respect to $b = 0^{\circ}$. This emission corresponds to gas between $l = 60^{\circ}$ and 91°, where the Local arm is seen along the line of sight (Cersosimo et al. 2009). Georgelin & Georgelin (1976) delineate for the first time the spiral structure of the Galaxy and

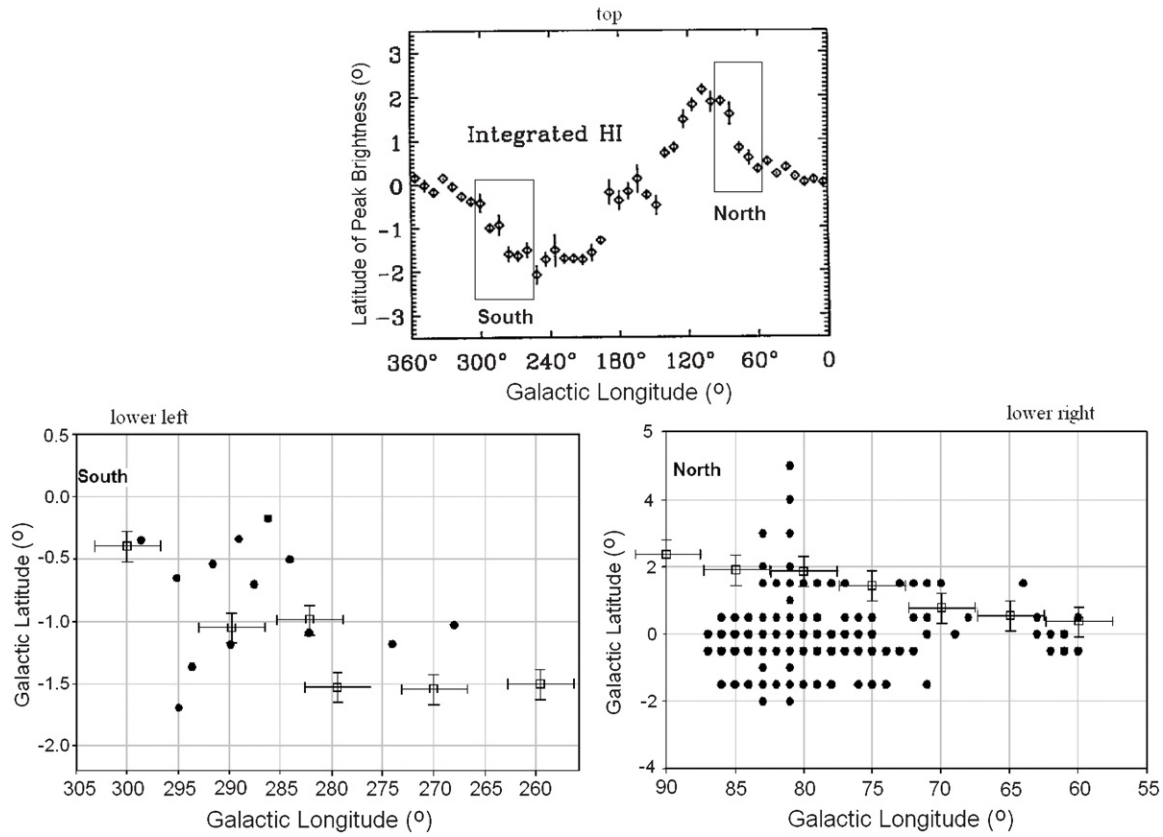

Figure 4. The upper panel shows the distribution of the integrated H I vs. Galactic longitude (Freudenreich et al. 1994). The superposed boxes show the regions considered in this paper for the southern and northern hemispheres. In the lower left panel, the dots represent our southern hemisphere sample, while the empty squares represent the integrated H I. The lower right panel is the same as the lower left panel, but for the northern hemisphere.

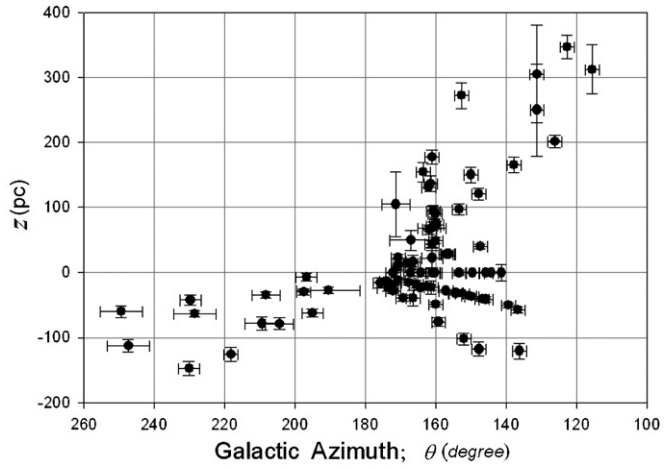

Figure 5. Vertical distribution of the H166α RRL emission as a function of Galactic azimuth. In the fourth quadrant ($\theta > 180^\circ$), the Galactic warp flares to $z \approx -100$ pc. In the first quadrant ($\theta < 180^\circ$), the Galactic warp flares to $z \approx +300$ pc.

show that it should has four spiral arms. Russeil (2003) and Russeil et al. (2007) using multiwavelength and observations of fainter and farther H II regions suggest a four-arm model to represent the grand design of our Galaxy. In this model, the Local arm is located between the two major spiral arms, Sag-Car and Perseus (see Figure 5 of Russeil et al. 2007, and Cersosimo et al. 2009), and the near side of the arm starts in the complex of North America and Pelican nebulae (Cersosimo et al. 2007).

The RRL emission between $150^\circ < \theta < 160^\circ$ and above $z = +100$ pc is associated with the Cygnus superbubble region which is populated by OB associations (Uyaniker et al. 2001). From the position of this structure, and toward lower azimuth angles, we can see a tilted distribution flaring above the Galactic plane. This suggests the presence of a warped structure. The ionized material located between $100^\circ < \theta < 130^\circ$ should belong to the Perseus arm.

7. GENERAL DISCUSSION

7.1. Neutral and Ionized Hydrogen

The H II gas is detected within a Galactic ring between $R = 8$ and 13 kpc, and the z-height distribution is established in Figures 3–5. We return to the discussion of Section 6.1. We note here that the H I data are widely distributed in z at larger R. The global characteristics of the outer-Galaxy H I layer was discussed by Burton & te Lintel Hekkert (1986). *The amplitude of the warp grows linearly, and is approximately equal in the two Galactic hemispheres, until about 12.8 kpc. At larger radii, the amplitude of the warp in the northern material continues to increase, until the sensitivity limits of the data are reached at $R \sim 20$ kpc, where the emission centroid lies some 3.2 kpc above the plane $b = 0^\circ$. The behavior of the warp in the southern hemisphere material is different: after reaching a maximum excursion of about 0.8 kpc below the Galactic equator at $R \approx 14.4$ kpc, the gas layer folds back again toward the equator at largest distances* (Burton 1988). Here, we compare our data with the distribution of H I emission located at similar galactic radii.

In Figure 6, we show the (θ, z) map of H I emission obtained at different Galactic radii adapted from the paper of

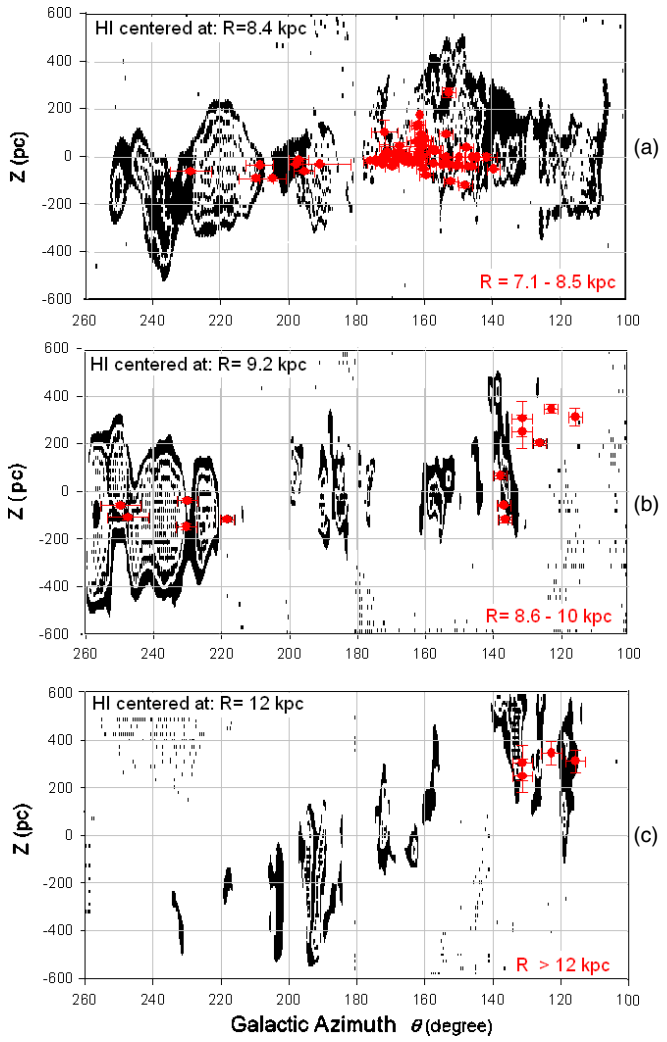

Figure 6. Contours of mean H I volume density ($0.30 < n_{\rm H} < 0.45$ cm^{-3}) in the (θ, z) plot for annuli centered at the indicated R and with $\Delta R = 500$ pc (Burton & te Lintel Hekkert 1986). The regions are centered at (a) $R = 8.4$ kpc, (b) $R = 9.2$ kpc, and (c) $R = 12.8$ kpc. The red dots show the H166α emission in the range $R = 7.1$–8.5 kpc, $R = 8.6$–10.0 kpc, and $R > 12$ kpc, respectively. (A color version of this figure is available in the online journal.)

Burton & te Lintel Hekkert (1986). The contours are drawn at atoms per cubic centimeter levels, indicated with white/black scale divisions which show the density levels between $0.30 < n_{\rm HI} < 0.45$ cm^{-3}. For comparison in Figure 6, the H166α data from Figure 5 are shown as red dots.

Figure 6(a) shows the atomic hydrogen distribution for $R = 8.4 \pm 0.5$ kpc and the H II distributed between 7.1 and 8.5 kpc. In the azimuth range between $\theta = 150°$ and 240°, the maximum intensity of the H I emission is tilted with respect to the Galactic $z = 0$ plane. This suggests that the effect of the warp is present near the solar circle in both quadrants. In the fourth quadrant, the H II is located below the Galactic plane. In the first quadrant, the H II layer is almost flat showing a similar distribution above and below $z = 0$. The gas located between $\theta = 140°$ and 180° defines the structure of the Local arm (Russeil 2003). From this feature, a structure emerges toward positive latitudes at $\theta \approx 160°$ and $z \approx +200$ pc. Another feature rises at $\theta \approx 150°$ to $z \approx +300$ pc. These structures seem to be associated with the Cygnus superbubble (Landecker 1984).

Figure 6(b) shows the atomic hydrogen distribution for $R = 9.2 \pm 0.5$ kpc combined with the H II gas located between distances $R = 8.6$ and 10 kpc. In the fourth quadrant, the maximum H I emission appears between $z \approx -400$ and +200 pc, while the ionized gas appears below the Galactic plane between $z \approx -180$ and -10 pc. In the first quadrant, the H I flares to positive z, between $z = -200$ and +400 pc with a maximum at $\theta = 140°$, while the ionized gas flares between the same z range but between $\theta \approx 115°$ and 138°.

In Figure 6(c), we see the H I gas at $R = 12 \pm 0.5$ kpc. The clumps of maximum H I density are tilted with respect to the $z = 0$ plane. They are from (θ, z) $\approx$ (230, -400) to (θ, z) $\approx$ (120, +500). In the fourth quadrant, the H I levels drop below $n_e = 0.45$ cm^{-3} and no H II regions are detected. In the first quadrant, the H166α emission is located between $z \approx +200$ and +400 pc and between $\theta \approx 130°$ and $\theta \approx 110°$. The ionized gas is located at $R \geqslant 12$ kpc, according to the kinematics distances this emission should belong to the Perseus arm.

In Figure 6(c), a source is located at (θ, z) = (115, +312) and it shows the largest radial velocity of the sample (Heiles et al. 1996). The kinematical distance of the source is $r = 14.6$ kpc. If we assume that the source is not contaminated by expansion process, this source is located in the Norma-Cygnus arm.

The three panels of Figure 6 suggest that an ionized warp is present in both quadrants. The tilt is seen in the Carina arm, and it is strongly present in the Perseus arm. The apparent inconsistencies between the results of the lower panels of Figure 4 and the panels of Figure 6 occur because the integrated H I maximum of Figure 4 corresponds to the overall gas outside the solar circle, while the H I gas shown in the panels of Figure 6 represents the most dense H I gas distribution for different distance ranges with respect to the Galactic center. We conclude that in the region near the solar circle, the high-density concentrations of the H I and H II gas distributions are similarly tilted, and both components show the sign of the warp. On the other hand, it is important to note that the measurements of Diplas & Savage (1991) at substantially lower values of $n_{\rm HI}$ permit us to probe the nature of the Galactic warp and the extension of the gas to large z in the outermost portions of the Galaxy.

The panels of Figure 6 suggest an asymmetry between the first and the fourth quadrants for the ionized warp. The H II is tilted with respect to the Galactic plane and in the fourth quadrant shows a truncation at $R \approx 10$ kpc. In contrast, in the first quadrant the truncation occurs at $12 \leqslant R < 16$ kpc. In addition, the flare of the fourth quadrant is smaller than the flare in the first one.

7.2. Stellar Warp

The behavior of the H166α distribution suggests that the ionized material may also trace the warp. From the point of view of the structure of the Milky Way (Georgelin & Georgelin 1976; Russeil 2003), the distribution of H166α line emission is consistent with the distribution of the spiral arms. In the fourth quadrant, the Carina arm is seen over 50° of longitude and between 8 and 9 kpc from the Galactic center. There is no evidence of spiral structure for the next few kpc behind the Carina arm. In the first quadrant, the line of sight runs along the Local arm, a structure distributed from longitudes 60° to 90°. It then goes through the Perseus arm at ~5 kpc from the Sun (Georgelin & Georgelin 1976; Russeil 2003).

Our data are probably dominated by the distribution of HMSS. From the comparison of the results of H I (Burton & te Lintel Hekkert 1986), we conclude that the HMSS disk and the high-density H I are similarly distributed and warped.

These components are truncated at some few kpc outside of the solar circle. The radial truncation of the stellar disk or simply a more rapid radial fall of the star formation mechanism as a consequence of lower gas density could be expected. Early search in the region of Puppis (Orsatti 1992) shows a significant number of faint OB stars at 0.5 kpc below the plane at $R = 12$ kpc. May et al. (1997, 2005) show the tilt of molecular gas from $R = 9$ to 15 kpc, and some clouds were found between 15 and 19 kpc. Carraro et al. (2005) and Pandey et al. (2006) report a tilted distribution of young stellar population in the third quadrant at distances $R \leqslant 13$ kpc. They suggest the existence of the Norma-Cygnus arm located below the Galactic plane, this being a clear effect of the Galactic warp.

Photometric observations obtained by Carney & Seitzer (1993) suggest the presence of a stellar population in the outer disk in the location of the southern warp. In addition, López-Corredoira et al. (2002) studied the existence of the warp in the Galactic stellar populations using star counts of old-population red clump giants selected from Two Micron All Sky Survey (2MASS) color–magnitude diagrams. The ratio of north and south Galactic star counts shows a sinusoidal behavior with longitude, and López-Corredoira et al. (2002) suggest the existence of the warp in the old stellar population whose amplitude is coincident with that of warped gas and young disk stars.

On the other hand, the distribution of OB stars (Miyamoto et al. 1988) shows an inclination of about 3° to the Galactic plane almost equal to the H II layer. Miyamoto et al. (1988) argued that OB stars follow the warp and found evidence that OB-type stars located in the Galactic ring from 8 to 9 kpc ($R_0 = 8.0$ kpc) have a systematic z-motion upward and downward from the Galactic plane for $l \leqslant 180°$ and for $l \geqslant 180°$, respectively.

Kaltcheva & Hilditch (2000) confirmed the existence of a young group of OB stars within $260° \lesssim l \lesssim 270°$ and for the distance range from the Sun of $0.3 \lesssim r \lesssim 2.5$ kpc. These stellar objects are spatially correlated with our RRL data around $l = 268°$ (source no. 9 in Table 2). However, young optical objects, such as young open clusters, stellar associations, and H II regions, show the same spatial distribution.

The dust layer, as revealed by *IRAS* fluxes follows the H I layer and shows the warp (Sodroski et al. 1987). The CO sources (May et al. 1997, 1988; Wouterloot et al. 1990) also show the signs of the warp, and furthermore with smaller thickness. The clouds show the warped shape and flaring thickness, as is seen for the outer-Galaxy H I gas layer. Comparison of the scale lengths of the H I and molecular clouds at $R \gtrsim 13.2$ kpc shows that the H I gas layer terminates less abruptly than the molecular cloud ensemble. May et al. (1997) and Wouterloot et al. (1990) claim that the absence of CO emission is not a consequence of instrumental limitations; evidently there are very few molecular clouds with embedded star formation at $R > 18.8$ kpc. This should be a result of the density distribution of the ISM. According to Bohigas (1988), a low molecular cloud-to-H I ratio results from the fact that external pressure is smaller than the critical pressure needed to convert diffuse clouds into molecular clouds. As a consequence, we expect H II at the same limits.

From a comparison of parameters of warped galaxies in the radio, and especially at visible wavelengths, Castro-Rodriguez et al. (2002) suggest that several mechanisms can be present in the warp formation at the same time. Olano (2004) proposes an interaction of HVCs produced by an event of mass transfer from the Magellanic Clouds. Also, using new H I data and numerical simulations, Levine et al. (2006) suggest that the tidal influence of the Magellanic Clouds creates distortions in the dark matter halo, which combine to produce a disk warp amplitude comparable to the H I observations. From these arguments and the discussion of Momany et al. (2006), it should be acceptable to suggest that both components, stellar and gas, are similarly distorted relative to the Galactic plane.

7.3. The Galactic Structure in the Fourth Quadrant

The Galactic longitude range observed here contains the Carina arm which is delineated over several kpc by standard radio and optical spiral tracers (Georgelin & Georgelin 1976; Russeil et al. 2007). In Figure 2, we show the results in a face-on view of the Galaxy, showing the distribution of the RRL in the (X, Y) plot. The Carina arm is also well defined by H I regions (Levine et al. 2006).

Figure 3 shows the vertical distribution of the H166α emission with Galactic radius. The ionized gas is located between $R = 7.1$ and 9.7 kpc and from $z \sim -150$ to -10 pc. Molecular clouds (Cohen et al. 1985; Grabelsky et al. 1987) lie within the region and are located slightly below the Galactic plane. The diffuse ionized gas and the CO emission are associated with regions of maximum H I density ($0.45 < n_e < 0.60$ cm^{-3}).

Figure 5 shows the distribution of the regions studied in the fourth and first quadrants in a (θ, z) plot. The Carina arm seems to be about 100 pc thick. The z position is about -100 pc at $\theta \approx 250°$ with the arm reaching the midplane at $\theta \approx 180°$. In the first quadrant, the ionized material is located between azimuths 180° and 110°, and is distributed both above and below the Galactic plane. Part of this emission corresponds to the Local arm (Russeil 2003), a feature thicker than the Carina arm, and does not exhibit any clear continuity from the Carina arm. Therefore, these two structures seem to be unrelated. This fact is in agreement with the four arms model proposed by Georgelin & Georgelin (1976) and Russeil (2003) for which the Carina arm cuts the solar circle at $l \sim 282°$. A further discussion about the structure of the Local arm is made by Cersosimo et al. (2009).

H I observations of McClure-Griffiths et al. (2004) reported a spiral arm located at 17 kpc from the Galactic center. This feature lies in the Galactic range of our survey. If H II regions are located in the spiral arm, we expect emission at the velocity range between 120 and 140 km s^{-1}, which is outside of the velocity range studied in this survey.

8. CONCLUSIONS

We have presented results of highly sensitive H166α observations from the fourth quadrant of the Galactic plane. Our conclusions are as follows.

1. The H166α emission observed traces the Carina arm. The ionized gas lies below the Galactic plane, descending from $z \approx -10$ to -150 pc between Galactic radii $R \approx 7.3$ and 9.7 kpc. From Figure 3, it is apparent that at larger galactocentric radii the shape of the distribution reflects that of the warp, with its z thickness increasing with increasing distance from the Galactic center.
2. Combining results for RRL emission in the first and fourth quadrants suggests that warped ionized gas exists in both quadrants. The phenomenon is more pronounced in the first quadrant, where the gas flares above the Galactic plane to $z \approx +350$ pc.
3. The ionized material is correlated with the maximum density of H I. Both components are tilted with respect

to the Galactic plane and show a truncation with increasing galactocentric distance. In the fourth quadrant, they are truncated at $R \approx 10$ kpc. In the first quadrant, they are truncated at $13 \lesssim R < 16$ kpc.

4. In the first quadrant, between $\theta = 140°$ and 180°, the ionized gas located between $z = -150$ and +150 pc traces the Local arm. A feature of ionized gas rises from this structure near $\theta = 160°$, probably associated with the Cygnus superbubble. Between Galactic azimuths $\theta = 100°$ and 150°, the RRL emission is located at $R > 10$ kpc and at high z; this material should be located at the Perseus arm.

We are grateful to Dr. Gerardo Morell who encouraged us to go forward with this project. We also are grateful to the Director and the staff of the Parkes Observatory (New South Wales, Australia) for their hospitality. J.C.C. gives special thanks to Dr. Federico Herrero of NASA and Dr. R. J. Muller, Chairman of the Department of Physics and Electronics and member of the Puerto Rico Space Grant (PRSG) Consortium, for encouraging this project. Our thanks to Dr. Christopher J. Salter, Tapasi Ghosh, and Marcel Agüeros for critical review of the paper. This research was supported by NASA Training Grant NNG05GG78H PRSG and NASA Cooperative Agreement NCC5-595 (PR NASA EPSCOR). We are also grateful to the program Advance-IT (NSF-SBE-0123645) for support of our students. This research has made use of NASA's Astrophysics Data System.

REFERENCES

Azcárate, I. N., Cersosimo, J. C., & Colomb, F. R. 1990, RevMexAA, 20, 75
Azcárate, I. N., Cersosimo, J. C., Wilkes, L. M., & Cordero, Y. A. 1997, Ap&SS, 253, 313
Bailin, J. 2003, ApJ, 583, L79
Barnes, D. G., et al. 2001, MNRAS, 322, 486
Battaner, E., Florido, E., & Sanchez-Saavedra, M. L. 1990, A&A, 236, 1
Bohigas, J. 1988, A&A, 205, 257
Brocklehurst, M., & Seaton, M. J. 1972, MNRAS, 157, 179
Burke, B. F. 1957, AJ, 62, 90
Burton, W. B. 1988, in Galactic and Extragalactic Radio Astronomy, ed. G. L. Verschuur & K. I. Kellermann (2nd ed.; Berlin: Springer), 295
Burton, W. B., & te Lintel Hekkert, P. 1986, A&AS, 65, 427
Carney, B. W., & Seitzer, P. 1993, AJ, 105, 2127
Carraro, G., Vázquez, R. A., Moitinho, A., & Baume, G. 2005, ApJ, 630, L153
Cash, W., Charles, P., Bowyers, S., Walter, F., Garmire, G., & Riegler, G. 1980, ApJ, 238, L71
Castro-Rodriguez, N., López-Corredoira, M., Sánchez-Saavedra, M. L., & Battaner, E. 2002, A&A, 391, 519
Caswell, J. L., & Haynes, R. F. 1987, A&A, 171, 261
Cersosimo, J. C., Azcárate, I. N., Colomb, F. R., & Hart, L. 1989, A&A, 349, 67
Cersosimo, J. C., Muller, R. J., Figueroa Vélez, S., Santiago Figueroa, N., Baez, P., & Testori, J. C. 2007, ApJ, 656, 248
Cersosimo, J. C., Muller, R. J., & Santiago Figueroa, N. 2009, ApJ, in press
Cohen, R. S., Grabelsky, D. A., Bronfman, L., Alvarez, H., & Thaddeus, P. 1985, ApJ, 290, L15
Comerón, F., Torra, J., & Gómez, A. E. 1998, A&A, 330, 975
Diplas, A., & Savage, B. D. 1991, ApJ, 377, 126
Djorgovski, S., & Sosin, C. 1989, ApJ, 341, L13
Fich, M., Blitz, L., & Stark, A. A. 1989, ApJ, 342, 272
Freudenreich, H. T., et al. 1994, ApJ, 429, L69
Gardner, F. F., Milne, D. K., Mezger, P. G., & Wilson, T. L. 1970, A&A, 7, 349
Georgelin, Y. M., & Georgelin, Y. P. 1976, A&A, 49, 57
Grabelsky, D. A., Cohen, R. S., Bronfman, L., Thaddeus, P., & May, J. 1987, ApJ, 315, 22
Heiles, C. 1994, ApJ, 436, 720
Heiles, C., Reach, W. T., & Koo, B. 1996, ApJ, 466, 191
Henderson, A. P., Jackson, P. D., & Kerr, F. J. 1982, ApJ, 263, 116
Huchtmeier, W. K., & Day, G. A. 1975, A&A, 41, 153
Kaltcheva, N. T., & Hilditch, R. W. 2000, MNRAS, 312, 753
Kerr, F. J. 1957, AJ, 62, 93
Kulkarni, S. R., & Heiles, C. 1988, in Galactic and Extragalactic Radio Astronomy, ed. G. L. Verschuur & K. I. Kellermann (2nd ed.; Berlin: Springer), 95
Kulkarni, S. R., Heiles, C., & Blitz, L. 1982, ApJ, 259, L63
Landecker, T. L. 1984, AJ, 89, 95
Levine, E. S., Blitz, L., & Heiles, C. 2006, Science, 312, 1773
Lockman, F. J. 1976, ApJ, 209, 429
Lockman, F. J., & Brown, R. L. 1978, ApJ, 222, 153
López-Corredoira, M., Betancort-Rijo, J., & Beckman, J. E. 2002, A&A, 386, 169
May, J., Alvarez, H., & Bronfman, L. 1997, A&A, 327, 325
May, J., Gyulbudaghian, A. L., & Alvarez, H. 2005, Afz, 48, 411
May, J., Murphy, D. C., & Thaddeus, P. 1988, A&AS, 73, 51
McClure-Griffiths, N. M., Dickey, J. M., Gaensler, B. M., & Green, A. J. 2004, ApJ, 607, L127
McGee, R. X., & Gardner, F. F. 1968, Aust. J. Phys., 21, 149
McKee, C. F., & Ostriker, J. P. 1977, ApJ, 218, 148
Mezger, P. G. 1978, A&A, 70, 565
Miyamoto, M., Yoshizawa, M., & Suzuki, S. 1988, A&A, 194, 107
Momany, Y., Zaggia, S., Gilmore, G., Piotto, G., Carraro, G., Bedin, L. R., & de Angeli, F. 2006, A&A, 451, 515
Olano, C. A. 2004, A&A, 423, 895
Oort, J. H., Kerr, F. J., & Westerhout, G. 1958, MNRAS, 118, 379
Orsatti, A. M. 1992, AJ, 104, 590
Osterbrock, D. E. 1989, Astrophysics of Gaseous Nebulae and Active Galactic Nuclei (Mill Valley, CA: Univ. Science Books), 24
Pandey, A. K., Sharma, S., & Ogura, K. 2006, MNRAS, 373, 255
Petuchowski, S. J., & Bennet, C. L. 1993, ApJ, 405, 591
Reid, M. J. 1993, ARA&A, 31, 345
Reynolds, R. J. 1983, ApJ, 268, 698
Rodger, A. W., Campbell, C. T., & Whiteoak, J. B. 1960, MNRAS, 121, 103
Roshi, D. A., & Anantharamaiah, K. R. 2001, ApJ, 557, 226
Russeil, D. 2003, A&A, 397, 133
Russeil, D., Adami, C., & Georgelin, Y. M. 2007, A&A, 470, 161
Sodroski, T. J., Dwek, E., Hauser, M. G., & Kerr, F. J. 1987, ApJ, 322, 101
Sparke, L. S., & Casertano, S. 1988, MNRAS, 234, 873
Staveley-Smith, L., et al. 1996, PASA, 13, 243
Tapia, M., Roth, M., Marraco, H., & Ruiz, M. T. 1988, MNRAS, 232, 661
Tsujimoto, M., Feigelson, E. D., Townsley, L. K., Broos, P. S., Getman, K. V., Wang, J., Garmire, G. P., & Baba, D. 2007, ApJ, 665, 719
Uyaniker, B., Fürst, E., Reich, W., Aschenbach, B., & Wielebinski, R. 2001, A&A, 371, 675
Voskes, T., & Burton, W. B. 2006, arXiv:astro-ph/0601653
Weinberg, M. D. 1998, MNRAS, 299, 499
Westerhout, G. 1957, Bull. Astron. Inst. Netherlands, 13, 201
Wilson, T. L., Mezger, P. G., Gardner, F. F., & Milne, D. K. 1970, A&A, 6, 364
Wouterloot, J. G. A., Brand, J., Burton, W. B., & Kwee, K. K. 1990, A&A, 230, 21